

Antibacterial effect, structural characterization, and some applications of silver chiral nano-flower sculptured thin films

Hadi Savaloni¹ · Fatemh Haydari-Nasab¹ · Abbas Abbas-Rohollahi²

Received: 20 May 2015 / Accepted: 25 May 2015 / Published online: 24 June 2015
© The Author(s) 2015. This article is published with open access at Springerlink.com

Abstract Silver chiral nano-flowers with 3-, 4-, and 5-fold symmetry were produced using oblique angle deposition method in conjunction with the rotation of sample holder with different speeds at different sectors of each revolution. X-ray diffraction, atomic force microscopy, and scanning electron microscopy were employed to obtain the nanostructure and morphology of the films. Their antibacterial, electrical, and hydrophobic properties were investigated. Antibacterial properties were investigated against a range of microorganisms including *Escherichia coli* ATCC 8739, *Staphylococcus aureus* ATCC 25923, and *Candida albicans* PTCC 5027. Electrical conductivity of these films relative to that of bulk sample is reduced by a factor of about 10^3 due to porosity, surface roughness, and anisotropic structure of these films. Hydrophobicity results show dependence on the symmetry of these chiral nano-flowers.

Keywords Silver chiral nano-flower · Thin film · Antibacterial · Electrical conductivity · Hydrophobicity

Introduction

The metallic nanostructures with specific properties dependent on their size and geometrical shape have created an interesting research environment for scientist in

different fields of application. In particular, noble metals (gold, silver, and copper) have found applications in optics [1, 2], electronic [3, 4], biomedicine and antibacterial activity [5–7], and quantum size domain [8].

This group of metallic nanostructures because of their ability in exhibiting localized surface Plasmon resonances (LSPR) has found many applications in biodetection [9]. LSPR excitation can considerably enhance the local electric field which is the main reported mechanism of surface-enhanced Raman spectroscopy (SERS) [10, 11].

Silver nanostructures, such as silver nanoparticles, provide a large surface-area-to-volume ratio and a high fraction of surface atoms [12], which enhance the antimicrobial activity of silver, even at low concentrations [13–18]. The antibacterial property of silver depends on the amount of silver and its reduction rate in the test environment. In recent years, silver coatings have shown to decrease bacterial adherence and growth in vitro [19–21]. The antibacterial activity of silver ions has been well established [22, 23], as lying in interactions with S, O, and N containing groups. However, the role of silver nanomaterials has not been as clearly determined and many contradictory findings are reported [24].

The cluster size, clusters cross-section, and its reaction rate with substrate have an important role in silver antibacterial activity [25]. Recent investigations have shown that enhanced antibacterial property can be achieved when silver nanocolumns/rods are used instead of normal silver thin films or silver nanoparticles. This is due to higher roughness of these structures and surface area ratio [26].

In addition, it is also well established that superhydrophobic surface can be achieved through combination of high surface roughness and low surface free energy [27–29]. A large number of physical techniques such as

✉ Hadi Savaloni
savaloni@khayam.ut.ac.ir

¹ Department of Physics, University of Tehran, North-Kargar Street, Tehran, Iran

² Department of Biology, University of Tehran, Enghelab Street, Tehran, Iran

lithographic patterning and etching, molding, and imprinting have been used to obtain rough surfaces in order to produce superhydrophobic surfaces [30–32]. On the other hand, direct deposition of micro/nanostructures of different materials such as metals [33], polymers [34], oxides [35], or carbon nanotubes [36] on substrates through chemical reactions and or assembly processes also have proved to show superhydrophobicity. Fan et al. [37] have found that as the height of the nanorod increased, the water contact angle of as grown Si nanorods decreased.

Layer-by-Layer (LbL) assembly was first introduced by G. Decher [38] in order to achieve superhydrophobic surface, as a versatile method to assemble layered nanostructures with tailored composition and architecture [39]. Savaloni and Esfandiari [40] achieved high degree of hydrophobicity by deposition of chiral-graded zigzag silver sculptured thin films. In recent years, oblique angle deposition (OAD) of thin films as a physical vapor deposition method has provided facilities for the production of variety of nanostructures with structural anisotropy which can be controlled by pre-design of the structure [41, 42].

OAD (incident angle $<85^\circ$) and glancing angle deposition (GLAD) (incident angle $>85^\circ$) methods together with the rotation of substrate about its surface normal can be used to produce differently shaped nanostructures such as chirals [43], zigzags [44], S-shaped, and other shapes [45]. Sculptured nanostructures (range in size between 1 and 100 nm) fabricated by these methods have many applications such as optical filters [46], photonic crystals [47], catalysts [48], magnetic storages [49], micro-batteries [50], bioscaffolds [51], and microchannels [52].

Oblique silver nanocolumns grown using OAD method without rotation of substrate have shown surface-enhanced Raman spectra (SERS) [53] and surface-enhanced fluorescence (SEF) [54] which can give useful and desired results in detection of minute amount of chemicals and viruses. Silver chiral nano-flowers with different symmetries have also shown a high degree of enhancement in obtaining surface Raman Spectra [11]. The structure of sculptured thin films (STFs) consists of rough surface with a much higher void fraction than the films produced using conventional deposition methods.

The use of OAD technique together with rotation of substrate and change of rotation rate during each revolution of the substrate by $2N$ ($N = 1-5$) provides facilities to produce nanostructures with N -fold symmetry called chiral nano-flowers [55].

In this work, we have used this technique and produced silver chiral nano-flowers with different symmetries and investigated their antibacterial, hydrophobicity, and electrical properties as well as structural characteristics. This work is to the best of our knowledge at the time of

submission, the first report on the above-mentioned properties of sculptured silver chiral nano-flowers with different orders of symmetry.

Experimental details

Silver (99.99 % purity) chiral nano-flower-shaped sculptured thin films with different symmetries were deposited on glass ($15 \times 15 \text{ mm}^2$ microscope slide) substrates by resistive evaporation from tungsten boats with a circular outlet of 6 mm in diameter at room temperature. An Edwards (Edwards E19 A3) coating plant with a base pressure of 2×10^{-7} mbar was used. The deposition angle was fixed at (80°) and a deposition rate of 2.5 \AA s^{-1} was chosen. In order to achieve a uniform deposition on the substrates, the distance between the evaporation source and the substrate was set at 30 cm. The deposition process was repeated a few times and the reproducibility of the results was confirmed. The movement of the stepper motor and its speed of revolution as well as facility for dividing each revolution to different sectors are controlled through interface to a computer in which the related software is written and installed [56].

Nano-flowers with 3-, 4-, and 5-fold symmetries were produced, considering that for an N -fold symmetry each revolution of the substrate holder should be divided to $2N$ sectors. In this work, in order to produce 3- and 4-fold symmetry nano-flower, the smaller sector was chosen as ($\theta_L = 24^\circ$) and for production of 5-fold symmetry, it was chosen as ($\theta_L = 18^\circ$) which rotates with a speed of $R_L = 0.0151$ (rev/s), while the other sectors size depends on the order of chosen symmetry and its speed (R_H) was chosen to be 32 times of R_L .

Prior to deposition, all substrates were ultrasonically cleaned in heated acetone then ethanol. The surface roughness of the substrates was measured by a Talysurf profilometer and AFM, and the rms substrate surface roughness R_q obtained using these methods was 0.3 and 0.9 nm, respectively.

The deposition rate was controlled using a quartz crystal monitor (Sigma Instruments, SQM-160, USA) positioned close to the substrate and at almost the same azimuthal angle as that of the substrate. This was corrected after obtaining the film thickness using field emission electron microscope (FESEM; Hitachi S-4100 SEM, Japan). FESEM samples were coated with a very thin layer of gold to prevent the charging effect. The surface physical morphology and roughness was obtained by means of atomic force microscope (AFM) (NT-MDT SOLVER, with a Si tip of 10 nm radius in contact mode) analysis.

Antibacterial activity of silver nano-flower thin films with different symmetries of 3-, 4-, and 5-folds against the *Escherichia coli* ATCC 8739, *staphylococcus aureus* ATCC 25923, and *Candida albicans* PTCC 5027 bacteria was studied using the so-called diffusion assay method. The bacteria were chosen because gram-negative bacteria are responsible for more than 80 % of all infections, with *E. coli* being responsible for more infections than all other genera combined. *S. aureus* and *C. albicans* were also utilized as representative members of gram-positive and fungal genera [57]. Among the bacteria studied, *E. coli* is gram-negative, whereas *S. aur* is gram-positive.

Prior to performing the microbiological experiment, all glass wares and samples were sterilized by autoclaving at 120 °C for 15 min. All films were cleaned by ethanol and acetone. For sterilization, they were placed into a sterilized Petri dish and irradiated by UVC lamp for 30 min. The microorganisms were cultured on a nutrient agar plate and incubated at 37 °C for 24 h. The cultured organisms were added in 10 ml saline solution to reach the concentration of bacteria to 10^8 colony forming units per milliliter (CFU/ml) corresponding to MacFarland scale. 100 μ l of the saline solution containing the microorganisms was added to nutrient agar plate and spread with a sterile cotton swab. Then for antibacterial test, each thin film was placed onto a cultured nutrient agar plate and incubated at 37 °C for 24 h. After 24 h area of inhibition zone of growth was measured.

Results and discussions

FESEM and AFM (nanostructure)

In our earlier work [58], we reported on the structural characteristics of similar thin films obtained using FESEM and AFM analysis. Since the results of this work are similar to those reported earlier, we do not see any point in repeating such results. However, it should be mentioned that in this work, the deposition angle was 80° and for the production of 5-fold symmetry nano-flower in this work we used $\theta_L = 18^\circ$, while in the earlier work $\theta_L = 24^\circ$ was applied. In order to get the structural information one may

Table 1 Results of grain/petal size, average surface roughness, and surface void fraction in the Ag chiral nano-flowers of different symmetries on glass substrates

Ag/glass nano-flower	D_{XRD} (nm)	D_{AFM} (nm)	R_{ave} (nm)	F_v (%)
3-fold	15.0	82.0	12.0	41.5
4-fold	17.0	70.0	15.9	32.4
5-fold	24.0	66.0	10.9	30.1

F_v is the surface void fraction obtained from 2D AFM images

consult Figs. 2 and 3 in [58]. In Table 1 we have included the results obtained for grain size and surface void fraction for the three types of silver chiral nano-flowers produced in this work.

Crystal structure

The XRD patterns of the samples produced in this work for three different symmetries are given in Fig. 1. Crystalline structure of the samples is consistent with the JCPDS card No: 04-0783. Zhou et al. [59] reported crystalline structure for their silver nanorod samples even when they reduced the substrate temperature to -40 °C.

Polycrystalline films deposited on substrates generally show preferred orientation, with a strength which depends on the deposition method, film material, and deposition conditions, including residual gas pressure. However, one should consider the fact that in case of oblique angle deposition or slanted films, the texture axis can be tilted out of the surface normal, and the evaluation of intensity distribution of various reflections for determining the texture can be completely misleading. In that case, the texture had to be analyzed by taking pole figures at fixed diffraction angle [31, 60]. Hence the procedure usually used for films deposited at normal deposition angle [61] cannot be applied to oblique angle or glancing angle deposited films. A program of work on this subject is currently under investigation in our group.

Crystallite size (coherently diffracting domains) D was obtained by applying the Scherrer formula [62] to measure the full width at half maximum (FWHM) of the dominant peak of silver nano-flower films [i.e., Ag(111)]. The results with 10 % accuracy are given in Table 1. The results show that the crystallite size (coherently diffracting domains) increases with increasing the order of symmetry of the chiral nano-flower.

Antibacterial property of Ag chiral nano-flowers

Nano-silver structures such as silver nanoparticles that have a large surface-to-volume ratio have shown a high degree of antibacterial property [63]. The antimicrobial activity of silver-based materials depends on the nanostructure that should provide a high surface-area-to-volume ratio and hence a high fraction of surface atoms [12, 26], which enhances the antibacterial property of silver. Pal et al. [64] investigated the antibacterial properties of silver nanoparticles with different shapes. They concluded that the differences in the observed trends in *E. coli* ATCC 8739 inhibition can be explained in terms of the percentage of active facets present in nanoparticles of different shapes. They also speculate that the action of silver nanoparticles is broadly similar to that of silver ion. It may be anticipated

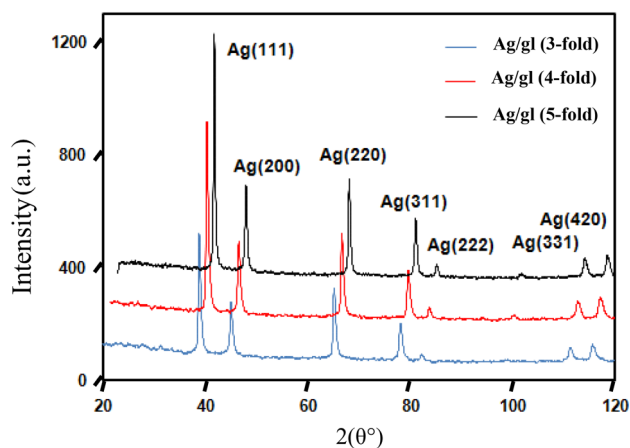


Fig. 1 XRD patterns of silver chiral nano-flower sculptured thin films with different symmetries

that a bacterial cell in contact with silver nanoparticles takes in silver ions, which inhibit a respiratory enzyme(s), facilitating the generation of reactive oxygen species and consequently damaging the cell [62]. It is also demonstrated that the reactivity of silver is favored by high-atom-density facets, such as {111} [15, 65, 66]. Hence it may reiterate that by increasing the surface-to-volume ratio and surface roughness of thin films, the probability of releasing silver atoms/ions in the medium increases, and since the Ag(111) facet consists of the maximum number of atoms in the silver structure, it should provide the highest antibacterial effect.

It is generally believed that heavy metals such as silver interact with the thiol groups of proteins that are important for the bacterial respiration and the transport of significant substances through the cell [67, 68]. In addition, silver ions can bind to the bacterial cell wall (slightly negative) and also alter the function of the bacterial cell membrane [69, 70]. Experimental evidence also proposes that silver ion interaction with bacteria causes DNA molecules to lose their replication capability [70]. Therefore, considering the structural and morphological results obtained for our silver chiral nano-flower thin films, presented in the preceding sections, we expect that our nano-sculptured thin films should show an enhanced antibacterial property compared to thin films deposited at normal incident angle.

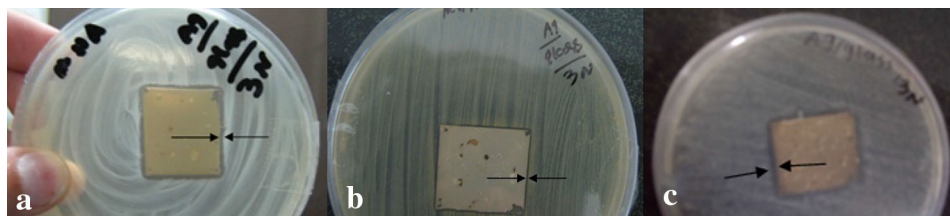


Fig. 2 Typical zone of inhibition (ZOI) for 3-fold symmetry silver chiral nano-flower for two different bacteria (*Escherichia coli* ATCC 8739 and *Staphylococcus aureus* ATCC 25923) and a fungus (*Candida albicans* PTCC 5027) after 24 h incubation

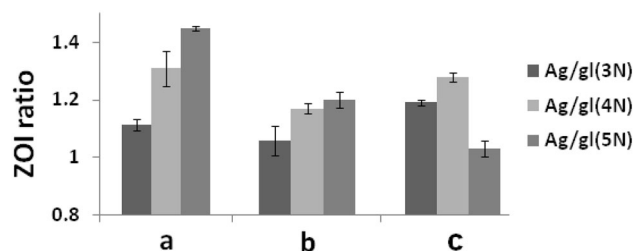


Fig. 3 The zone of inhibition for silver chiral nano-flower films of different symmetries against different test strains is compared after 24 h incubation; a *Escherichia coli* ATCC 8739, b *Staphylococcus aureus* ATCC 25923, c *Candida albicans* PTCC 5027

Figure 2 shows typical zone of inhibition (ZOI) for 3-fold symmetry silver chiral nano-flower on Petri dish for two different bacteria and a fungus, namely *E. coli* ATCC 8739, *S. aur* ATCC 25923, and *C. albicans* PTCC 5027 after 24 h incubation. ZOI was recorded as the ratio of the area of antibacterial activity to the area of the sample.

In Fig. 3, the ZOI obtained for silver chiral nano-flower films of different symmetries against different test strains are compared. In Fig. 3, columns indicated by (1) are the results of *E. coli* ATCC 8739, columns indicated by (2) are for *S. aur* ATCC 25923, and columns indicated by (3) are for *C. albicans* PTCC 5027, respectively. It can be seen that in case of the first two bacteria, the 5-fold symmetry nano-flower antibacterial effect dominates the other two structures. This may be due to the high intensity of (111) orientation of this sample, as discussed in “Crystal structure” and higher surface-to-volume ratio due to increased number of petals in this film. However, for *C. albicans* PTCC 5027, the 4-fold symmetry nano-flower is more active than the other two structures. In addition it should also be mentioned that all three nanostructures used in this work have more antibacterial effect on *E. coli* ATCC 8739, relative to the *S. aur* ATCC 2592. This is because the *E. coli* ATCC 8739 is a gram-negative bacteria.

Electrical property of Ag nano-flowers

In this section, we discuss the results obtained from the measurements of the dc resistance. In order to investigate the influence of possible (low frequency) charging effects

Table 2 Results of conductivity measurement for Ag/glass nano-flower sculptured thin films with different symmetries in S/cm unit

	Ag/glass (3-fold)	Ag/glass (4-fold)	Ag/glass (5-fold)
0°	7.83×10^3	5.81×10^3	6.11×10^3
45°	7.03×10^3	5.85×10^3	6.34×10^3
90°	7.54×10^3	5.51×10^3	6.09×10^3
135°	6.92×10^3	6.12×10^3	6.64×10^3
Anisotropy between 0° and 90°	0.0188	0.0265	0.0016

at the electrical contacts and leads, current–voltage (I–V) curves were recorded, scanning the voltage both in increasing and decreasing increments. In order not to heat up the samples, during the measurements, the current was kept low enough. A linear I–V curve was obtained, independent of the scan direction, and there was no indication of hysteresis effect. In order to investigate the anisotropy effect in our samples, the I–V curves measurements were also carried out in four different directions on the samples in 45° increments. The average values of conductivity for three silver chiral nano-flower samples with different symmetries are given in Table 2. Results in Table 2 show that conductivity of each sample changes with the direction of measurement, hence showing the effect of anisotropy in the structure of chiral nano-flower silver thin films as expected. The anisotropy in the data was obtained using.

$$\text{Anisotropy} = \frac{A_x - A_y}{A_x + A_y}$$

where x and y are related to two measurements at x and y directions, namely 0° and 90° measurements. It can be seen that the sample with 4-fold symmetry shows the highest anisotropy, this is expected since the petals of nano-flower with 4-fold symmetry are positioned with exactly 90 degree spacing between them and may have introduced the bundling-like effect which usually occurs in the oblique deposition technique into the structure of the grown thin film.

In addition, we can also observe that the sample with 3-fold symmetry shows the highest conductivity and the sample with 4-fold symmetry shows the lowest conductivity. The reasons for these observations may be explained as follows; it is well known that the conductivity of a sample depends on the number of grain boundaries, surface roughness, impurities, film cross-section, and number and size of voids in the electron path that cause scattering of electrons resulting in the loss of energy. As expected from the design of the chiral nano-flower structures, the 3-fold symmetry consists of largest grains/petals and the 5-fold symmetry contains smallest grains/petals (Table 1, column 3), hence considering the element of size, it can be concluded that the 3-fold symmetry sample should have the highest conductivity. However, the difference between grain/petal sizes of 4-fold and 5-fold symmetry samples

may not be significant enough for causing the different conductivities obtained for these two samples. The sample with 4-fold symmetry has the highest surface roughness (Table 1, column 4). Therefore, it may cause a high degree of electron scattering from the surface which in turn decreases the film conductivity. In addition as our electrical measurements at different directions mentioned above showed this sample has the highest anisotropy which we related this phenomenon to the bundling-like effect in this sample, hence this may also be another parameter in the decreased conductivity of this sample relative to 3-fold and 5-fold symmetry samples. The size and number of voids (grain boundaries) are other parameters that we should consider with regard to the changes in the conductivity of the samples. As mentioned in the experimental section, the sections with high rotation rate (i.e., voids) for 3- and 4-fold symmetry nano-flowers were produced with 24° angles, while for 5-fold symmetry, this was 18° (a reduction by 25 %). Hence we expect that the size of voids in the 5-fold symmetry sample be smaller than the other two samples, while the number of voids (grain boundaries) between petals of the chiral nano-flower in 5-fold symmetry is increased. Therefore, in general, as the symmetry order increases, the θ_h section of the growing film becomes smaller and the growing sculpture thin film seems to resemble a circle. In particular, in our 5-fold symmetry chiral nano-flower case, we also reduced the section (θ_h) relative to 4-fold symmetry sample. This can be the reason for higher conductivity of this film relative to the 4-fold symmetry sample which has larger voids between petals.

Hydrophobicity effect of silver chiral nano-flower sculptured thin films

It is well established that superhydrophobic surface can be achieved through combination of high surface roughness and low surface free energy [27–29]. Since the surfaces of chiral nano-flowers produced in this work consist of pointed petals and recesses between petals, it is expected to be rougher than thin films produced using normal deposition procedure, hence they may show higher hydrophobicity effect. The results of surface roughness shown in Table 1 and results of hydrophobicity test on our silver chiral nano-flower sculptured thin films with 3-, 4-, and

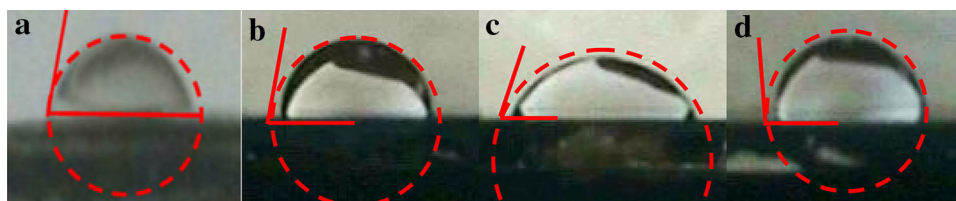


Fig. 4 Contact angles for water droplets on, **a** 300 nm silver thin film deposited at normal angle to the substrate without rotation of substrate holder; **b** silver chiral nano-flower with 3-fold symmetry; **c** silver

chiral nano-flower with 4-fold symmetry; **d** silver chiral nano-flower with 5-fold symmetry

Table 3 Contact angle for Ag/glass nano-flower sculptured thin films with different symmetries

Structure	Ag/gl (normal)	Ag/gl (3-fold)	Ag/gl (4-fold)	Ag/gl (5-fold)
Contact angle	69°	85°	72°	106°

5-fold symmetries and a silver film of 300 nm thickness deposited under conventional condition of normal incidence angle shown in Fig. 4 are compared. It can be observed that the contact angle for all chiral nano-flower samples is greater than that obtained for the film deposited at normal incidence angle (Table 3). Obviously, these results cannot be accepted as superhydrophobic achievement, but they indicate that their surface hydrophobicity is increased relative to the conventionally deposited silver film. 4-fold symmetry silver chiral nano-flower shows smaller contact angle than those obtained for 3- and 5-fold symmetry silver chiral nano-flowers. This can be due to increased symmetry axes in this sample, though the film surface roughness for this film is greater than 3- and 5-fold symmetry nano-flowers. As discussed throughout this paper, the morphology (length and shape) of nanocolumns as well as interspaces and air diffusion between nanocolumns change. These variations of structural parameters are the main factors for the increase of contact angle [71]. Hence in this work, we have achieved enhanced hydrophobic surface (i.e., for 3- and 5-fold symmetry chiral nano-flowers) by engineering the sample surface via sculptured thin film deposition to produce chiral nano-flowers.

Conclusions

We produced and obtained the antibacterial effect, electrical, and hydrophobicity properties of silver chiral nano-flowers with three different symmetries by applying oblique angle deposition method in conjunction with the rotation of sample holder with different speeds at different sectors of each revolution. Nanostructure and morphology of the produced samples were obtained using

XRD, AFM, and FESEM. Antibacterial properties were investigated against a range of microorganisms including *E. coli* ATCC 8739, *S. aureus* ATCC 25923, and *C. albicans* PTCC 5027. It was observed that the 5-fold symmetry chiral nano-flower antibacterial effect is more pronounced than 3- and 4- fold symmetry chiral nano-flowers in acting on *E. coli* ATCC 8739 and *S. aur* ATCC 25923, which can be related to its crystallographic structure [high intensity of (111) orientation] and higher surface-to-volume ratio. Electrical conductivity of these films relative to that of bulk sample is reduced by a factor of about 10^3 due to porosity, surface roughness, and anisotropic structure of these films. Hydrophobicity results showed dependence on the symmetry of chiral nano-flower.

Acknowledgments This work was carried out with the support of the University of Tehran and the Iran National Science Foundation (INSF). HS is grateful to the Centre of Excellence for Physics of Structure and Microscopic Properties of Matter, Department of Physics, University of Tehran for partial support of this work.

Open Access This article is distributed under the terms of the Creative Commons Attribution 4.0 International License (<http://creativecommons.org/licenses/by/4.0/>), which permits unrestricted use, distribution, and reproduction in any medium, provided you give appropriate credit to the original author(s) and the source, provide a link to the Creative Commons license, and indicate if changes were made.

References

- Feng, J., Zhao, X., Liu, B., Zhou, X.: Microstructural characterization and optical polarization of glass with needle-like micro-nano silver oriented arrangement. *Opt. Commun.* **281**, 5041–5044 (2008)
- Chu, T.C., Liu, W.C., Tsai, D.P.: Enhanced resolution induced by random silver nanoparticles in near-field optical disks. *Opt. Commun.* **246**, 561–567 (2005)
- Park, K., Seo, D., Lee, J.: Conductivity of silver paste prepared from nanoparticles. *Coll. Surf. A.* **313**, 351–354 (2008)
- Alqudami, A., Annapoorni, S., Sen, P., Rawat, R.S.: The incorporation of silver nanoparticles into polypyrrole: conductivity changes. *Synth. Met.* **157**, 53–59 (2007)
- Chen, C.Y., Chiang, C.L.: Preparation of cotton fibers with antibacterial silver nanoparticles. *Mater. Lett.* **62**, 3607–3609 (2008)



6. Nakamura, H., Tanaka, M., Shinohara, S., Gotoh, M., Karube, I.: Development of a self-sterilizing lancet coated with a titanium dioxide photocatalytic nano-layer for self-monitoring of blood glucose. *Biosens. Bioelectron.* **22**, 1920–1925 (2007)
7. Beyth, N., Yudovin-Farber, I., Bahir, R., Domb, A.J., Weiss, E.I.: Antibacterial activity of dental composites containing quaternary ammonium polyethylenimine nanoparticles against *Streptococcus mutans*. *Biomaterials* **27**, 3995–4002 (2006)
8. Jiang, L., Wang, W., Wu, D., Zhan, J., Wang, Q., Wu, Z., Jin, R.: Preparation of silver quantum dots embedded water-soluble silica/PAAc hybrid nanoparticles and their bactericidal activity. *Mater. Chem. Phys.* **104**, 230–234 (2007)
9. Alivisatos, P.: The use of nanocrystals in biological detection. *Nat. Biotechnol.* **22**, 47–52 (2004)
10. Willets, K.A., Van Duyne, R.P.: Localized surface plasmon resonance spectroscopy and sensing. *Annu. Rev. Phys. Chem.* **58**, 267–297 (2007)
11. H Savaloni and R Babaei, Surface-enhanced Raman spectroscopy and structural characterization of Ag/Cu Chiral Nano-flower Sculptured Thin films. *Appl. Surf. Sci.* (2013) in print
12. Ichinose, N., Ozaki, Y., Kashu, S.: *Superfine particle technology*. Springer, New York (1992)
13. Lee, H.J., Yeo, S.Y., Jeong, S.H.: Antibacterial effect of nano-sized silver colloidal solution on textile fabrics. *J. Mater. Sci.* **38**, 2199–2204 (2003)
14. Lok, C.N., Ho, C.M., Chen, R., He, Q.Y., Yu, W.Y., Sun, H., Tam, P.K.H., Chiu, J.F., Che, C.M.: Proteomic analysis of the mode of antibacterial action of silver nanoparticles. *J. Proteome Res.* **5**, 916–924 (2006)
15. Morones, J.R., Elechiguerra, J.L., Camacho, A., Holt, K., Kouri, J.B., Ramirez, J.T., Yacaman, M.J.: The bactericidal effect of silver nanoparticles. *Nanotechnology* **16**, 2346–2353 (2005)
16. Maneerung, T., Tokura, S., Rujiravanit, R.: Impregnation of silver nanoparticles into bacterial cellulose for antimicrobial wound dressing. *Carbohydr. Polym.* **72**, 43–51 (2008)
17. Mahapatra, S.S., Karak, N.: Silver nanoparticle in hyperbranched polyamine: synthesis, characterization and antibacterial activity. *Mater. Chem. Phys.* **112**, 1114–1119 (2008)
18. Xu, K., Wang, J.X., Kang, X.L., Chen, J.F.: Fabrication of antibacterial monodispersed Ag–SiO₂ core-shell nanoparticles with high concentration. *Mater. Lett.* **63**, 31–33 (2009)
19. Leung, J.W.C., Lau, G.T.C., Sung, J.J.Y., Costerton, J.W.: Decreased bacterial adherence to silver-coated stent material: an in vitro study. *Gastrointest. Endosc.* **38**, 338–340 (1992)
20. Liedberg, H., Lundberg, T.: Silver alloy coated catheters reduce catheter-associated bacteriuria. *Urol. Res.* **25**, 937–952 (1991)
21. Boswald, M., Girisch, M., Greil, J., Spies, T., Stehr, K., Krall, T., Guggenbichler, J.P.: Antimicrobial activity and biocompatibility of polyurethane and silicone catheters containing low concentrations of silver: a new perspective in prevention of polymer-associated-foreign-body-infections. *Zentralbl. Bakteriol.* **283**, 187–200 (1995)
22. Slawson, R.M., Van Dyke, M.I., Lee, H., Trevors, J.T.: Germanium and silver resistance, accumulation, and toxicity in microorganisms. *Plasmid* **27**, 72–79 (1992)
23. Russell, A.D., Chopra, I.: Understanding antibacterial action and resistance. Hemel Hempstead, chapter 3. Hertfordshire: Ellis Horwood, UK (1996)
24. Marambio-Jones, C., Hoek, E.M.V.: A review of the antibacterial effects of silver nanomaterials and potential implications for human health and the environment. *J. Nanopart. Res.* **12**, 1531–1551 (2010)
25. Silvestry-Rodriguez, N., Sicairos-Ruelas, E.E., Gerba, C.P., Bright, K.R.: Silver as a disinfectant. *Rev. Environ. Contam. Toxicol.* **191**, 23–45 (2007)
26. Akhavan, O., Ghaderi, E.: Capping antibacterial Ag nanorods aligned on Ti interlayer by mesoporous TiO₂ layer. *Surf. Coat. Technol.* **203**, 3123–3128 (2009)
27. Wenzel, R.N.: Resistances of solid surfaces to wetting by water. *J. Ind. Eng. Chem.* **28**, 988–994 (1936)
28. Cassie, A.B.D., Baxter, S.: Wettability of porous surfaces. *Trans. Faraday Soc.* **40**, 546–551 (1944)
29. Zhao, N., Shi, F., Wang, Z., Zhang, X.: Combining layer-by-layer assembly with electrodeposition of silver aggregates for fabricating superhydrophobic surfaces. *Langmuir* **21**, 4713–4716 (2005)
30. Nosonovsky, M., Bhushan, B.: Biomimetic Superhydrophobic Surfaces: multiscale Approach. *Nano Lett.* **7**, 2633–2637 (2007)
31. Cho, W.K., Choi, I.S.: Fabrication of hairy polymeric films inspired by geckos: wetting and high adhesion properties. *Adv. Funct. Mater.* **18**, 1089–1096 (2008)
32. Winkleman, A., Gotesman, G., Yoffe, A., Naaman, R.: Immobilizing a drop of water: fabricating highly hydrophobic surfaces that pin water droplets. *NanoLett.* **8**, 1241–1245 (2008)
33. Larmour, I.A., Bell, S.E.J., Saunders, G.C.: Sheets of large superhydrophobic metal particles self assembled on water by the cheerios effect. *Angew. Chem. Int. Ed.* **47**, 5043–5045 (2007)
34. Balu, B., Breedveld, V., Hess, D.W.: Fabrication of “roll-off” and “sticky” superhydrophobic cellulose surfaces via plasma processing. *Langmuir* **24**, 4785–4790 (2008)
35. Namavar, F., Cheung, C.L., Sabirianov, R., Mei, W.N., Zeng, X.C., Wang, G., Haidar, H., Garvin, K.L.: Lotus effect in engineered zirconia. *Nano Lett.* **8**, 988–996 (2008)
36. Pastine, S.J., Pkawa, D., Kessler, B., Rolandi, M., Llorente, M., Zettl, A., Frechet, J.M.: A facile and patternable method for the surface modification of carbon nanotube forests using perfluoroarylazides. *J. Am. Chem. Soc.* **130**, 4238 (2008)
37. Fan, J.G., Dyer, D., Zhang, G., Zhao, Y.P.: Nanocarpet effect: pattern formation during the wetting of vertically aligned nanorod arrays. *Nano Lett.* **4**, 2133–2138 (2004)
38. Decher, G., Hong, J.D.: Buildup of ultrathin multilayer films by a self-assembly process: consecutive adsorption of anionic and cationic bipolar amphiphiles on charged surfaces. *Makromol. Chem. Macromol. Symp.* **46**, 321–327 (1991)
39. Decher, G., Schlenoff, J.B.: *Multilayer thin films: sequential assembly of nanocomposite materials*. Wiley, Weinheim (2002)
40. Savaloni, H., Esfandiari, A.: Fabrication, characterization and some applications of graded chiral zigzag shaped nano-sculptured silver thin films. *Appl. Surf. Sci.* **257**, 9425–9434 (2011)
41. Robbie, K., Brett, M.J.: Chiral sculptured thin films. *Nature (London)* **384**, 616 (1996)
42. Robbie, K., Brett, M.J.: Sculptured thin films and glancing angle deposition: growth mechanics and applications. *J. Vac. Sci. Technol. A* **15**, 1460–1465 (1997)
43. Dick, B., Brett, M.J., Smy, T.: Controlled growth of periodic pillars by glancing angle deposition. *J. Vac. Sci. Technol. B* **21**, 23–28 (2003)
44. Kesapragada, S.V., Victor, P., Nalamasu, O., Gall, D.: Nano-spring pressure sensors grown by glancing angle deposition. *Nano Lett.* **6**, 854–857 (2006)
45. Messier, R., Venugopal, V.C., Sunal, P.D.: Origin and evolution of sculptured thin films. *J. Vac. Sci. Technol. A* **18**, 1538–1545 (2000)
46. Wu, Q., Hodgkinson, I.J., Lakhtakia, A.: Circular polarization filters made of chiral sculptured thin films: experimental and simulation results. *Opt. Eng.* **39**, 1863–1868 (2000)
47. Kennedy, S., Brett, M.J., Miguez, H., Toader, O., John, S.: Optical properties of a three-dimensional silicon square spiral photonic crystal. *Photon. Nanostruct. Fundam. Appl.* **1**, 37–42 (2003)



48. Harris, K.D., McBride, J.R., Nietering, K.E., Brett, M.J.: Fabrication of porous platinum thin films for hydro- carbon sensor applications. *Sens. Mater.* **13**, 225–234 (2001)
49. Dick, B., Brett, M.J., Smy, T.J., Freeman, M.R., Malac, M., Egerton, R.F.: Periodic magnetic microstructures by glancing angle deposition. *J. Vac. Sci. Technol. A* **18**, 1838–1844 (2000)
50. Fleischauer, M.D., Li, J., Brett, M.J.: Columnar thin films for three-dimensional microbatteries. *J. Electrochem. Soc.* **156**, A33–A36 (2009)
51. Demirel, M.C., So, E., Ritty, T.M., Naidu, S.H., Lakhtakia, A.: Fibroblast cell attachment and growth on nanoengineered sculptured thin films. *J. Biomed. Mater. Res. B Appl. Biomater.* **81**, 219–223 (2007)
52. Harris, K.D., Brett, M.J., Smy, T.J., Backhouse, C.: Microchannel surface area enhancement using porous thin films. *J. Electrochem. Soc.* **147**, 2002–2006 (2000)
53. Suzuki, M., Maekita, W., Wada, Y., Nagai, K., Nakajima, K., Kimura, K., Fukuoka, T., Mori, Y.: Ag nanorod arrays tailored for surface-enhanced Raman imaging in the near-infrared region. *Nanotechnology* **19**, 265304 (2008)
54. Abdulhalim, I., Karabchevsky, A., Patzig, C., Rauschenbach, B., Fuhrmann, B., Eltzov, E., Marks, R., Xu, J., Zhang, F., Lakhtakia, A.: Surface-enhanced fluorescence from metal sculptured thin films with application to biosensing in water. *Appl. Phys. Lett.* **94**, 063106 (2009)
55. Zhao, Y.P., Ye, D.X., Wang, G.C., Lu, T.M.: Novel nano-column and nano-flower arrays by glancing angle deposition. *Nano Lett.* **2**, 351–354 (2002)
56. Savaloni, H., Babaei, F., Song, S., Placido, F.: Characteristics of sculptured Cu thin films and their optical properties as a function of deposition rate. *Appl. Surf. Sci.* **255**, 8041–8047 (2009)
57. Davis, C.P., Wagle, N., Anderson, M.D., Warren, M.M.: Bacterial and fungal killing by iontophoresis with long-lived electrodes. *Antimicrob. Agents Chemother.* **35**, 2131–2134 (1991)
58. Savaloni, H., Haydari-Nasab, F., Malmir, M.: Nano-structural characteristics and optical properties of silver chiral nano-flower sculptured thin films. *Appl. Surf. Sci.* **257**, 9044–9055 (2011)
59. Zhou, Q., Li, Z., Yang, Y., Zhang, Z.: Arrays of aligned, single crystalline silver nanorods for trace amount detection. *J. Phys. D Appl. Phys.* **41**, 152007 (2008)
60. Savaloni, H., Moradi, G.R., Player, M.A.: Texture development and residual stress in UHV evaporated silver films on glass substrates as a function of substrate temperature. *Vacuum* **77**, 245–257 (2005)
61. Savaloni, H., Gholipour-Shahraki, M., Player, M.A.: A comparison of different methods for X-ray diffraction line broadening analysis of Ti and Ag UHV deposited thin films: nanostructural dependence on substrate temperature and film thickness. *J. Phys. D Appl. Phys.* **39**, 2231–2247 (2006)
62. Savaloni, H., Modiri, F.: Surface nano-structural modifications and characteristics in nitrogen ion implanted W as a function of temperature and N⁺ energy. *Appl. Surf. Sci.* **253**, 1135–1142 (2006)
63. Jeon, H.J., Yi, S.C., Oh, S.G.: Preparation and antibacterial effects of Ag–SiO₂ thin films by sol–gel method. *Biomaterials* **24**, 4921–4928 (2003)
64. Pal, S., Tak, Y.K., Song, J.M.: Does the antibacterial activity of silver nanoparticles depend on the shape of the nanoparticle? a study of the gram-negative bacterium *Escherichia coli*. *Appl. Env. Mic.* **73**, 1712–1720 (2007)
65. Ajayan, P.M., Marks, L.D.: Quasimelting and phases of small particles. *Phys. Rev. Lett.* **60**, 585–587 (1988)
66. Hatchett, D.W., White, H.S.: Electrochemistry of sulfur adlayers on the low-index faces of silver. *J. Phys. Chem.* **100**, 9854–9859 (1996)
67. Cho, K.H., Park, J.E., Osaka, T., Park, S.G.: The study of antimicrobial activity and preservative effects of nanosilver ingredient. *Electrochim. Acta* **51**, 956–960 (2005)
68. Ivan, S., Branka, S.S.: Silver nanoparticles as antimicrobial agent: a case study on *E. coli* as a model for Gram-negative bacteria. *J. Coll. Interface Sci.* **275**, 177–182 (2004)
69. Percival, S.L., Bowler, P.G., Russell, D.: Bacterial resistance to silver in wound care. *J. Hosp. Infect.* **60**, 1–7 (2005)
70. Feng, Q.L., Wu, J., Chen, G.Q., Cui, F.Z., Kim, T.N., Kim, J.O.: A mechanistic study of the antibacterial effect of silver ions on *Escherichia coli* and *Staphylococcus aureus*. *J. Biomed. Mater. Res.* **52**, 662–668 (2000)
71. Cheng, Y.H., Chou, C.K., Chen, C., Cheng, S.Y.: Critical length of nanowires for hydrophobic behavior. *Chem. Phys. Lett.* **397**, 17–20 (2004)

